Fossilized high pressure from the Earth's deep interior: The coesite-in-diamond barometer

Nikolai V. Sobolev*, Boris A. Fursenko*, Sergei V. Goryainov*, Jinfu Shu†, Russell J. Hemley†, Ho-kwang Mao†‡, and Francis R. Boyd†

*Institute of Mineralogy and Petrography, Russian Academy of Sciences Siberian Branch, Novosibirsk, 630090, Russia; and †Geophysical Laboratory and Center for High Pressure Research, Carnegie Institution of Washington, 5251 Broad Branch Road NW, Washington, DC 20015-1305

Contributed by Ho-kwang Mao, August 23, 2000

Mineral inclusions in diamonds provide an important source of information about the composition of the continental lithosphere at depths exceeding 120–150 km, i.e., within the diamond stability field. Fossilized high pressures in coesite inclusions from a Venezuela diamond have been identified and measured by using laser Raman and synchrotron x-ray microanalytical techniques. Micro-Raman measurements on an intact inclusion of remnant vibrational band shifts give a high confining pressure of 3.62 (±0.18) GPa. Synchrotron single-crystal diffraction measurements of the volume compression are in accord with the Raman results and also revealed direct structural information on the state of the inclusion. In contrast to olivine and garnet inclusions, the thermoelasticity of coesite favors accurate identification of pressure preservation. Owing to the unique combination of physical properties of coesite and diamond, this ''coesite-in-diamond'' geobarometer is virtually independent of temperature, allowing an estimation of the initial pressure of Venezuela diamond formation of 5.5 (±0.5) GPa.

Specimens of Earth materials from great depths often contain mineralogical or textural clues, such as metastable high-pressure polymorphs or characteristic mineral assemblages implicating their high-pressure genealogy (1–3). The actual *pressure*, however, is seldom preserved and observed. For such observations, the sample must be retained in a strong container with appropriate relative thermoelastic properties, and nondestructive analytical techniques must be developed to probe the fossilized pressure condition *in situ* in the container. Diamond is the strongest possible container. Infrared absorption spectroscopy has been used as the probe for fluid inclusions in diamond (4), and high residual pressures have been reported on the basis of infrared spectra of quartz and CO_2 inclusions in the material (5, 6). In these studies, bulk spectra of diamond and numerous microscopic inclusions were measured; pressures and phases of different inclusions were not determined individually. Herein, we present direct measurements of pressures up to 3.6 GPa in individual coesite inclusions in diamond, a thermoelastic couple most favorable for pressure preservation. We use micro-Raman- and micro-single-crystal x-ray diffraction techniques to probe the pressure of each inclusion separately and precisely. Application to coesite inclusions in diamond from Venezuela provides a determination of the pressure-temperature (*P-T*) conditions of its formation.

Diamond and its inclusions contain rich information about the petrogenesis and geochemistry of the Earth's deep interior (7, 8). Although coesite- and diamond-bearing rocks (9–12) undoubtedly have a high-pressure origin, individually, coesite and diamond cover a wide *P-T* domain of stability (13, 14) that precludes their use as a precise and accurate geobarometer, because they give only a lower bound on the pressure of formation. In many cases, much higher pressures are suggested (15) based on mineral equilibria data, including SiO_2 solubility in garnets (16) or K_2O solubility in clinopyroxenes (17). Such compositional geobarometers, however, depend on experimental calibrations that have been limited to simple systems quite different from natural compositions. Coelastic mechanical couples of inclusions in diamond provide a way to pinpoint the pressure along the *P-T* path of the rock. Owing to its very high bulk and shear moduli (K and μ, respectively), diamond can preserve compressed mineral inclusions at an effective pressure up to several gigapascals without plastic deformation. The preserved pressure depends on the difference in compressibility and expansivity of the host diamond relative to the inclusion. Many minerals found as inclusions in diamonds exhibit thermoelasticity that preserves either no pressure (e.g., garnet; refs. 18 and 19) or low pressure (e.g., olivine; ref. 19) after the diamond has been transported to the Earth's surface. The coesite-in-diamond couple has many unique advantages. The high compressibility and low thermal expansivity of coesite provide the opportunity to preserve the maximum pressure with little dependence on the trapping temperature. The compositional simplicity of coesite avoids the problems of chemical variability in olivine, garnet, and fluid inclusions, because the measured properties (i.e., vibrational bands or lattice parameters) shift with composition as well as pressure.

Two separate coesite inclusions, a small (60-μm) triangular single crystal and a larger (200-μm) one, were singled out in a 2-mm diamond crystal from Venezuela for microanalyses (Fig. 1). No cracks or other evidence of plastic deformation, other than strong tangential tension, were detected in the diamond adjacent to the small inclusion, indicating nearly perfect preservation of the enclosure condition. Conversely, small cracks and strongly deformed regions in the diamond adjacent to the large inclusion indicate possible loss of pressure. In contrast to many previous determinations, the host diamond above the inclusion was not removed by polishing to bring the coesite grains to the surface; rather, the inclusions were analyzed *in situ*, deep inside the host diamond for maximum protection of any fossilized pressure. The nondestructive micro-Raman spectroscopy and microcrystal x-ray diffraction probes provide excellent spatial (±2-μm) and pressure (±0.1-GPa) resolution. Both Raman and x-ray results reveal ultrahigh fossilized pressures of the two inclusions.

Micro-Raman spectroscopy has been used widely for inclusion identification and often yields decisive information on the nature of the inclusion and the mineral species (18–21). Some typical mineral inclusions in diamonds such as olivine and garnet exhibit Raman shifts indicating their compressed state (18, 19). Notably, some of the first micro-Raman studies of solid inclusions were carried out on coesite (e.g., refs. 21 and 22), but evidence for confining pressure was not reported. Both practically and conceptually, the technique parallels the micro-Raman method developed for studying Earth and planetary materials in high-

Abbreviation: *P-T*, pressure-temperature.

‡To whom reprint requests should be addressed. E-mail: mao@gl.ciw.edu.

The publication costs of this article were defrayed in part by page charge payment. This article must therefore be hereby marked "*advertisement*" in accordance with 18 U.S.C. §1734 solely to indicate this fact.

Article published online before print: *Proc. Natl. Acad. Sci. USA*, 10.1073/pnas.220408697. Article and publication date are at www.pnas.org/cgi/doi/10.1073/pnas.220408697

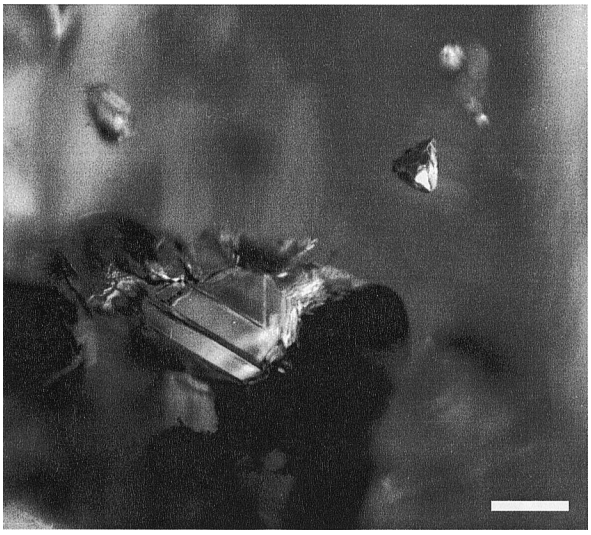

Fig. 1. Coesite inclusions in the Venezuela diamond studied by the Raman spectroscopy. Larger grain (close to the center) is surrounded by cracks, but around the smaller triangular grain (upper right side,) there are no cracks. The oval grain that is out of focus (upper left corner) is clinopyroxene as was confirmed by Raman spectroscopy. The presence of clinopyroxene inclusion confirms a coesite eclogite assemblage of the diamond. The diamond size is about 2 mm. (Bar = 100 μm.)

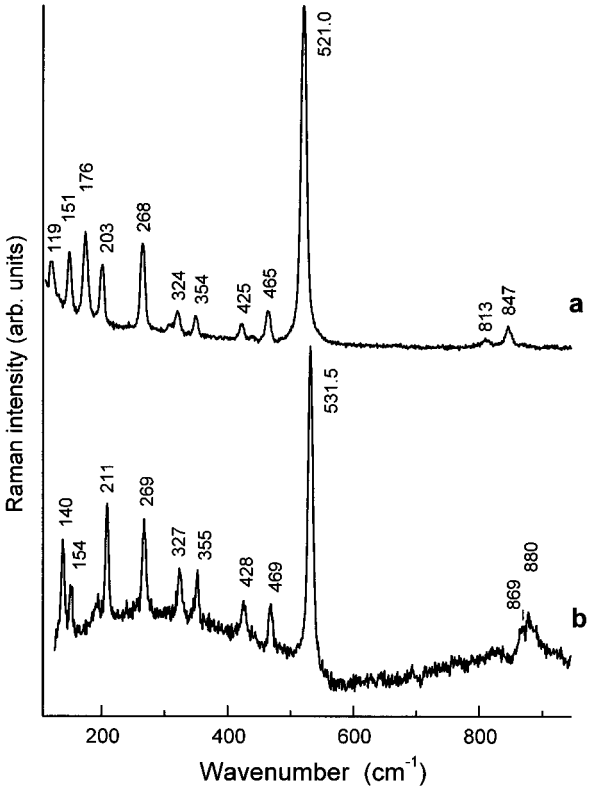

Fig. 2. Raman spectra in the range 100–900 cm^{-1} determined with the OMARS 89 System. (*a*) Synthetic coesite. (*b*) Small triangular coesite inclusion in diamond (compare with Fig. 1). The pressure was determined from the shift of the 521-cm^{-1} peak according to $\nu = 520.6 + 2.9(1) * P$ (GPa) (27).

pressure diamond cells (23–26); both techniques use microscope objectives to focus the excitation laser to micrometer-sized beam waists and to collect Raman signals with confocal or crossline optics from three-dimensional micrometer-sized volumes of samples encapsulated in millimeter-thick diamonds. The pressure dependence of the Raman spectrum of coesite has been measured up to 40 GPa in diamond cells (27). The most intense band at 521 cm^{-1} has a strong, characteristic pressure shift of 2.9 ($\pm$0.1) cm^{-1}/GPa. This band is used for pressure measurements in the present study. Raman spectra (Fig. 2) obtained from seven different points of the small coesite inclusion gave a uniform Raman shift of the 521-cm^{-1} band, $\Delta\nu = 10.5$ ($\pm$0.5) cm^{-1}, which corresponds to 3.62 ($\pm$0.18) GPa. Likewise, 12 different points of the large coesite inclusion gave a uniform Raman shift of $\Delta\nu =$ 8.0 ($\pm$0.5) cm^{-1} or 2.76 ($\pm$0.18) GPa.

Micro-single-crystal x-ray diffraction of the inclusions provides detailed structural and strain information on the state of the inclusion (Fig. 3). The energy dispersive single-crystal technique was developed originally at the beamline X17C of the National Synchrotron Light Source for high-pressure diamond-cell investigations. The technique has been used for studying 10-μm-sized single crystals of hydrogen at high pressure (28, 29), 220-nm-diameter single-crystal fiber in glass capillaries (30), and submicrometer-thick magnetite lamellae in olivine phenocrysts from ultrahigh-pressure rocks (31). It was used in the present work for studying the same two coesite inclusions in diamond (Fig. 1). The coesite diffraction peaks are sharp (Fig. 3), and rocking curves are tight (e.g., 0.5° for the 130 diffraction), indicating homogeneously strained single crystals. The orientation matrices of the two coesite inclusions were determined separately and found to be unrelated to each other or to the host diamond. Measurements of 56 diffraction peaks of the small coesite single crystal give the lattice parameters $a = 7.033$ ($\pm$0.009) Å, $b = 12.308$ ($\pm$0.004) Å, $c = 7.115$ ($\pm$0.005) Å, $\beta =$ 120.6 ($\pm$0.1)°, and $V = 529.8$ ($\pm$0.1) Å^3; likewise, 97 diffraction peaks for the large coesite give $a = 7.039$ ($\pm$0.001) Å, $b = 12.306$ ($\pm$0.001) Å, $c = 7.136$ ($\pm$0.004) Å, $\beta = 120.3$ ($\pm$0.2)°, and $V =$ 533.6 ($\pm$0.2) Å^3. By using the pressure-volume equation of state of coesite determined in diamond cells up to 25 GPa (32, 33), the corresponding pressures are 3.44 ($\pm$0.10) and 2.62 ($\pm$0.10) GPa for the small and large crystals, respectively.

Pressures from the x-ray and Raman measurements are in good agreement. The lower value of 2.76 ($\pm$0.18) GPa for the large inclusion indicates a partial leak as evident from small cracks in the diamond container. The fully preserved inclusion pressure (P_i) is taken to be 3.62 ($\pm$0.18) GPa from the small inclusion. This pressure reflects the originally higher pressure (P_t) and temperature (T_t) conditions under which the inclusions were trapped, with the volume of the inclusion $V_i(P_t,T_t)$ equal to the volume of the hole in the diamond $V_d(P_t,T_t)$. The latter is confirmed by the crystal faces of coesite inclusions, which are parallel to the faces of the host diamond. These are typical features of negative crystals and confirm the syngenetic nature of the coesite inclusions (11). Subsequently, the pressure readjusted from P_t to P_i as the diamond was brought to ambient conditions.

This change in the inclusion-container system is readily determined from the thermoelastic properties of coesite and diamond and may be divided into two steps (see Table 1): (*i*) isothermal decompression at constant temperature, T_t, and (*ii*) temperature decrease from T_t to 298 K at constant external pressure (P_o = 0.1 MPa). Retracing these two steps brings us from the present interior inclusion pressure of P_i at $T_o = 298$ K back to the original equilibrium pressure of P_t at T_t. The isothermal decompression consists of two terms. The first term simply results from the compressional volume difference between the diamond and coesite: $V(P_t) = V_d(P_t) - V_c(P_t)$, i.e., considering the diamond and its hole to be decompressed uniformly to P_0. This analysis gives $P_{t0} = 5.0$ GPa as a "zero approximation." The second term corresponds to nonuniform elastic deformation in the diamond under the internal inclusion

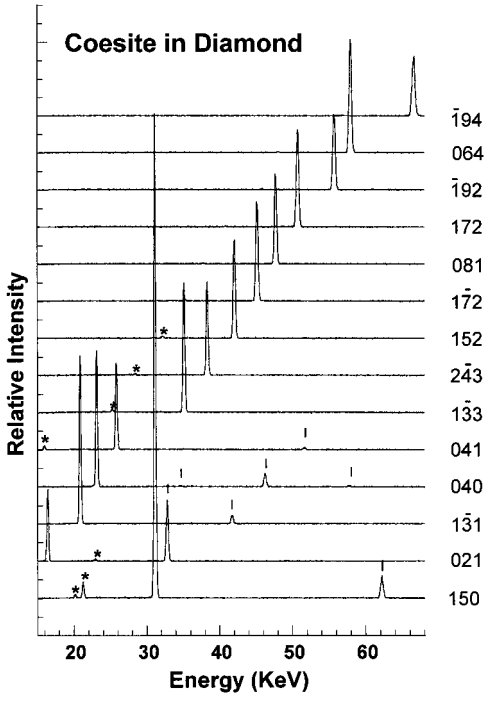

Fig. 3. Single-crystal energy dispersive x-ray diffraction patterns measured on the small coesite inclusion, collected at fixed $2\theta = 10.002°$ ($E\,d = 70.094$ keV-Å; 1 eV = 1.602×10^{-19} J) and room temperature. Reflections of 14 different *h k l*, randomly picked from a total of 56, are shown. Each reflection was obtained at a distinct χ, ω diffraction direction dictated by the orientation matrix of the single crystal. Short vertical ticks mark the overtones (*nh nk nl*), and the asterisks mark Ge detector escape peaks.

pressure P_i and external pressure P_0. From elasticity theory, this term can be expressed to a first approximation as $3/4[(P_i - P_o)/\mu_d]$ (compare ref. 19) and increases pressure by 0.8 GPa. The net result of the isothermal decompression gives $P_t = 5.8$ GPa. Correction for the small thermal expansivity difference between coesite and diamond (0.3 GPa) decreases P_t to 5.5 GPa. It is interesting to note that, as opposed to other minerals such as olivine or garnet, the thermal expansivity of coesite is even smaller than that of diamond, which results in some additional compression of the inclusion in diamond on cooling at constant pressure. Summarizing all errors (e.g., the present measurements and thermoelastic parameters), the resulting uncertainty in P_t is estimated to be $\pm$ 0.5 GPa.

The general range of equilibration temperatures is rather broad for 33 garnet + pyroxene pairs of inclusions: 1,000–1,300°C with an average of about 1200°C (34). Among them are five diamonds each containing garnet, pyroxene, and coesite as a set of multiple inclusions. Use of the Fe-Mg exchange equilibrium thermometer (35) gives a similar temperature range: 1,130–1,300°C with an average of about 1210°C. The differences in estimated solubility limit of *K* in clinopyroxenes included in diamonds from different occurrences may also correlate with different pressure/depth for diamond formation. The pressure of 5.5 GPa for coesite-bearing Venezuela diamond is consistent with the high estimate solubility limit of *K* in clinopyroxenes from diamonds of this occurrence (34).

Beginning with the first identification of a coesite eclogite assemblage represented by the set of coesite, garnet, and omphacite multiple inclusions in two Yakutian diamonds (36), the number of documented coesite-bearing diamonds from different occurrences is continuously increasing and reached about 150 samples at the end of 1999 (37–40). SiO_2 closely associated with magnesiowüstite was identified by Harte *et al.* (41) and postulated to be of lower mantle origin. However, no information is available in regard to the phase represented by SiO_2 (quartz, coesite, or stishovite). Despite this uncertainty, this finding of SiO_2 looks very promising and requires detailed characterization of this unusual suite of diamonds for the purpose of applying the independent coesite-in-diamond barometer. Raman shift measurements for probable coesite may provide a wider pressure range up to the coesite-stishovite equilibrium boundary (see Fig. 4). The Argyle mine E type diamond inclusions are other good candidates to have been formed within the range of pressures higher than those found for most peridotitic inclusions. The abundance of coesite-bearing diamonds (about 20%), high equilibration *T*, high *K* in clinopyroxenes, and Na in garnets (42, 43) allow the prediction of higher initial pressure of Argyle diamond formation compared with Venezuela.

The estimate of 5.5 GPa and ≈1,200°C was obtained for the crystallization of the Venezuelan diamond plots in the diamond stability field, close to the diamond-graphite equilibrium bound-

Table 1. Thermoelastic properties of diamond and coesite

Parameter	Designation	Units	Diamond	Coesite
Bulk modulus	$K_o = -V(dP/dV)_T$	GPa	442†	99.8‡
Its pressure derivative	$K'_o = (dK_o/dP)_T$		4†	6.3‡
Its temperature derivative	$(dK_o/dT)_P$	GPa/K	−0.0188†	−0.020§
Shear modulus	μ_d	GPa	538†	
Thermal expansivity	$\alpha = 1/V(dV/dT)_P = a + bT + cT^2 + dT^3$	1/K		
Coefficients in equation for α	$a*10^6$		6.828¶	5.43‖
	$b*10^6$		0.042¶	0.005‖
	$c*10^{10}$		−0.309¶	0
	$d*10^{15}$		8.88¶	
Raman shift vs. pressure	$d\nu/dP$	cm^{-1}/GPa		2.9 (±0.1)††

The $\Delta V/V$ term at constant temperature, for both diamond and coesite, can be found from a simple Murnaghan equation of state, $P = K'_o/K_o[(V_o/V)^{Ko} + 1]$, where $K(P) = K_o + K'_oP$ and $K(T) = K_o + (dK/dT)dT$. The temperature dependence of the diamond bulk modulus is below the error limits and can be effectively neglected. The pressure dependence of thermal expansivity may also be neglected, especially taking into account the very small difference in thermal expansion between coesite and diamond.

†Ref. 51.
‡Refs. 32 and 33.
§Ref. 53.
¶Ref. 54.
‖Ref. 52.
††Ref. 27.

GEOLOGY

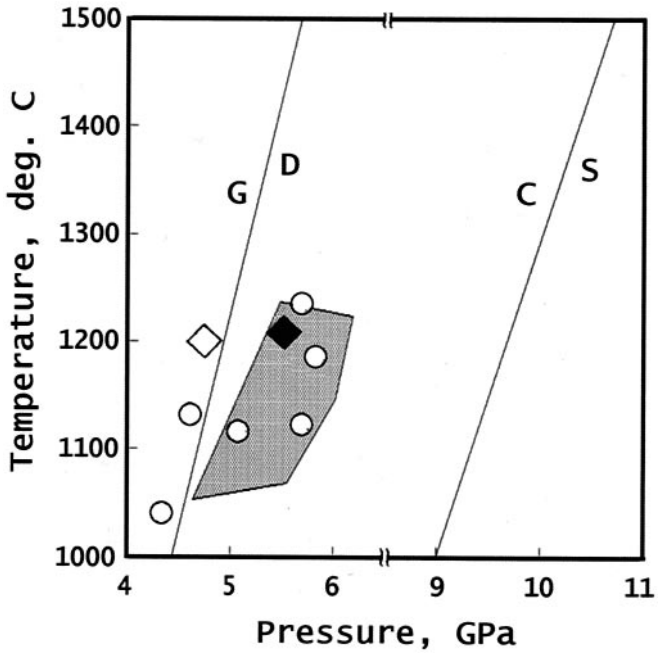

Fig. 4. A comparison of the *P-T* estimate made for the compression of coesite inclusions in a Venezuelan diamond (solid diamond) with estimates made by several methods for a variety of peridotitic diamonds. Open diamond, compression of olivine inclusions (19). Shaded field, touching diamond inclusions, mostly orthopyroxene + garnet, with one extreme point omitted (44). Open circles, perdotite xenoliths containing diamond, worldwide (garnet + olivine/PBKN thermobarometer, discussed by Pearson *et al.*, ref. 45). Data for diamondiferous peridotites are from Dawson and Smith (55), Boyd and Finnerty (56), Shee *et al.* (57), and Viljoen *et al.* (23). The graphite-diamond boundary (G/D) is from Kennedy and Kennedy (14). The coesite-stishovite boundary (C/S) is from Zhang *et al.* (58).

ary. This point for an eclogitic diamond is close to *P-T* estimates obtained for a variety of peridotitic inclusion assemblages and diamond-bearing peridotite xenoliths (Fig. 4). Methods used to estimate crystallization pressures of peridotitic diamonds include application of the Al-enstatite barometer (e.g., ref. 44) as well as the compression of olivine inclusions (19). The relative paucity of majorite-bearing and of other ultradeep diamonds as well as the data in Fig. 4 suggest that most macrodiamonds have originated in a depth zone that is within a GPa of the diamond-graphite stability boundary.

The pressure of the diamond stability boundary in Archaean cratons, the sources of most diamonds, is near 4.5 GPa (140 km) as defined by the intersection of the diamond-graphite curve with the cratonic geotherm. Both macrocrystalline diamonds and graphite are largely restricted to lithosphere within or peripheral to cratons for reasons that are not understood at present (45). The occurrence of diamond at depth in cratons, however, tends to be limited by the presence of nondiamondiferous high-temperature peridotites that are enriched in Fe and Ti and that have asthenospheric trace element signatures. These compositions may limit diamond crystallization, because they are more oxidized than overlying lithosphere (46). Equilibration pressures estimated for high-temperature peridotites are of the order of 6 GPa (190 km). The interval between 4.5 and 6 GPa has been termed the "diamond window" (47) for prospecting purposes and seems to be reflected in the concentration of *P-T* points shown in Fig. 4.

Nucleation effects may also have operated in the crystallization of natural macrodiamonds and may be an additional cause of the cluster of points in Fig. 4. Syntheses of coarse diamonds (>3 mm) are commonly carried out by relatively slow growth of seeds at pressures within a few tenths of a gigapascal of the diamond stability boundary. Experiments at greater pressures produce rapid nucleation and growth of large numbers of smaller diamonds (48). A majority of natural microdiamonds might thus have a deeper origin, where relatively abundant nuclei have formed and depleted the carbon reservoir.

In conclusion, the combination of laser Raman and synchrotron x-ray microanalytical techniques has allowed the unambiguous identification of high fossilized pressure in individual inclusions of mantle samples recovered at the Earth's surface. Moreover, the fossilized pressure of the inclusion and the thermoelasticity of the host-inclusion couple provide a highly accurate barometer. The ability to use the compression of coesite inclusions to estimate the pressure of crystallization of diamonds of eclogitic paragenesis fills a long-standing need and forms an important complement to the barometers that have been used for peridotitic diamonds. Significantly, coesite inclusions have been identified in more than 15 different diamond localities (49), and coesite eclogite paragenesis is confirmed to be a significant inclusion suite in diamond. It is likely that careful studies will result in coesite inclusion detection in at least some diamonds from any given kimberlite or lamproite occurrence (12, 37, 49, 50). The Mir pipe in Yakutia may be considered an instructive example. Despite the minor relative proportion of diamonds containing eclogitic inclusions for this pipe (1–10% by different estimations), five diamonds in total containing coesite have been documented among 70 diamonds with inclusions of eclogitic minerals that have been studied (39, 49). Thus, coesite inclusions in diamonds should not be considered very rare and thus may be useful as a geobarometer for diamonds from occurrences worldwide.

We thank A. I. Turkin for synthesis of coesite crystals; G. N. Kuznetsov, C. T. Prewitt, and Y. I. Shurin for stimulating discussions; and R. M. Hazen, C. T. Prewitt, and G. Snyder for review of this paper. X-ray diffraction measurements were performed at the X17C beamline of the National Synchrotron Light Source. This work is partially supported by the National Science Foundation and the Department of Energy.

1. Dobrzhinetskaya, L., Green, H. W. & Wang, S. (1996) *Science* **271,** 1841–1845.
2. Hacker, B. R., Sharp, T., Zhang, R. Y., Liou, J. G. & Hervig, R. L. (1997) *Science* **278,** 702–704.
3. McCammon, C. A., Hutchison, M. & Harris, J. (1997) *Science* **278,** 434–436.
4. Navon, O., Hutcheon, I. D., Rossman, G. R. & Wasserburg, G. J. (1988) *Nature (London)* **335,** 384–389.
5. Navon, O. (1991) *Nature (London)* **353,** 746–748.
6. Schrauder, M. & Navon, O. (1991) *Nature (London)* **365,** 42–44.
7. Cartigny, P., Harris, J. W. & Javoy, M. (1998) *Science* **280,** 1421–1423.
8. Haggerty, S. E. (1999) *Science* **285,** 851–853.
9. Chopin, C. (1984) *Contrib. Mineral. Petrol.* **86,** 107–118.
10. Sobolev, N. V. & Shatsky, V. S. (1990) *Nature (London)* **343,** 742–746.
11. Sobolev, N. V. (1974) *Deep-Seated Inclusions in Kimberlites and the Problem of Upper Mantle Composition* (Nauka, Novosibirsk, Russia).
12. Meyer, H. O. A. (1987) in *Mantle Xenoliths*, ed. Nixon, P. H. (Wiley, New York), pp. 501–523.
13. Bohlen, S. R. & Boettcher, A. L. (1982) *J. Geophys. Res.* **87,** 7073–7078.
14. Kennedy, C. S. & Kennedy, G. C. (1976) *J. Geophys. Res.* **81,** 2467–2470.
15. Haggerty, S. E. (1994) *Earth Planet. Sci. Lett.* **122,** 57–69.
16. Gurney, J. J. (1989) in *Kimberlites and Related Rocks*, ed. Ross, J. (Blackwell, Scientific, Oxford), Geological Society of America Special Publication No. 14, pp. 935–965.
17. Harlow, G. E. (1997) *Am. Mineral.* **82,** 259–269.
18. Liu, L. G., Mernagh, T. P. & Jaques, A. L. (1990) *Contrib. Mineral. Petrol.* **105,** 156–161.
19. Izraeli, E., Wilcock, I. C. & Navon, O. (1998) in *Extended Abstracts of Seventh Kimberlite Conference, Cape Town*, eds. Gurney, J. J., Gurney, J. L., Pascoe, M. D. & Richardson, S. H. (Red Roof Design, Cape Town, South Africa), pp. 355–357.

20. Harris, J. W. (1968) *Ind. Diamond Rev.* **28,** 402–410.
21. Boyer, H., Smith, D. C., Chopin, C. & Lasnier, B. (1985) *Phys. Chem. Minerals* **12,** 45–48.
22. Gillet, P., Ingrin, J. & Chopin, C. (1984) *Earth Planet. Sci. Lett.* **70,** 426–436.
23. Vijoen, K. S., Swash, P. M., Otter, M. L., Schulze, D. J. & Lawless, P. J. (1992) *Contrib. Mineral. Petrol.* **110,** 133–138.
24. Hemley, R. J., Bell, P. M. & Mao, H. K. (1987) *Science* **237,** 605–612.
25. Kingma, K. J., Cohen, R. E., Hemley, R. J. & Mao, H. K. (1995) *Nature (London)* **374,** 243–245.
26. Chou, I. M., Blank, J., Goncharov, A. F., Mao, H. K. & Hemley, R. J. (1998) *Science* **281,** 809–812.
27. Hemley, R. J. (1987) in *High-Pressure Research in Mineral Physics*, eds. Manghnani, M. H. & Syono, Y. (Terra Scientific, Tokyo), pp. 347–359.
28. Mao, H. K., Jephcoat, A. P., Hemley, R. J., Finger, L. W., Zha, C. S., Hazen, R. M. & Cox, D. E. (1988) *Science* **239,** 1131–1134.
29. Loubeyre, P., LeToullec, R., Hausermann, D., Hanfland, M., Hemley, R. J., Mao, H. K. & Finger, L. W. (1996) *Nature (London)* **383,** 702–704.
30. Skelton, E. F., Ayers, J. D., Qadri, S. B., Moulton, N. E., Cooper, K. P., Finger, L. W., Mao, H. K. & Hu, J. Z. (1991) *Science* **253,** 1123–1125.
31. Zhang, R. Y., Shu, J., Mao, H. K. & Liou, J. G. (1999) *Am. Mineral.* **84,** 564–569.
32. Levien, L. & Prewitt, C. T. (1981) *Am. Mineral.* **66,** 324–333.
33. Hemley, R. J., Jephcoat, A. P., Mao, H. K., Ming, L. C. & Manghnani, M. N. (1988) *Nature (London)* **334,** 52–54.
34. Sobolev, N. V., Yefimova, E. S., Channer, D. M. D., Anderson, P. F. N. & Barron, K. M. (1998) *Geology* **26,** 971–974.
35. Ellis, D. J. & Green, D. H. (1979) *Contrib. Mineral. Petrol.* **71,** 13–22.
36. Sobolev, N. V., Yefimova, E. S., Koptil, V. I., Lavrent'ev, Y. G. & Sobolev, V. S. (1976) *Dokl. Akad. Nauk SSSR* **230,** 1442–1444.
37. Daniels, L. R. M. & Gurney, J. J. (1999) in *Proceedings of the VIIth International Kimberlite Conference*, eds. Gurney, J. J., Gurney, J. L., Pascoe, M. D. & Richardson, S. H. (Red Roof Design, Cape Town, South Africa), Vol. 1, pp. 134–142.
38. Bulanova, G. P., Griffin, W. L., Kaminsky, F. V., Davies, R., Spetsius, Z., Ryan, C. G., Andrew, A. & Zakharchenko, O. D. (1999) in *Proceedings of the VIIth International Kimberlite Conference*, eds. Gurney, J. J., Gurney, J. L., Pascoe, M. D. & Richardson, S. H. (Red Roof Design, Cape Town, South Africa), Vol. 1, pp. 49–56.
39. Bulanova, G. P., Shelkov, D., Milledge, H. J., Haury, E. H. & Smith, C. B. (1999) in *Proceedings of the VIIth International Kimberlite Conference*, eds. Gurney, J. J., Gurney, J. L., Pascoe, M. D. & Richardson, S. H. (Red Roof Design, Cape Town, South Africa), Vol. 1, pp. 57–65.
40. Sobolev, N. V., Taylor, L. A., Zuev, V. M., Bezborodov, S. M., Snyder, G. A., Yefimova, E. S. & Sobolev, V. S. (1998) *Geologiya i Geofizika* **39,** 1667–1678; trans. *Russian Geol. Geophys.* **39,** 1653–1663 (Russian).
41. Harte, B., Harris, J. W., Hutchinson, M. T., Watt, G. R. & Wilding, M. C. (1999) in *Mantle Petrology: Field Observations and High Pressure Experimentation: A Tribute to Francis R. (Joe) Boyd*, eds. Fei, Y., Bertka, C. M. & Mysen, B. O. (Geochem. Soc., Houston), pp. 125–153.
42. Jaques, A. L., Hall, A. F., Sheraton, J. W., Smith, C. B., Drew, R. M., Foudoulis, C. & Ellingsen, K. (1989) in *Kimberlites and Related Rocks*, ed. Ross, J. (Geol. Soc. Australia, Special Publication), Vol. 14, pp. 966–989.
43. Sobolev, N. V., Galimov, E. M., Smith, C. R., Yefimova, E. S., Maltsev, K. A., Hall, A. E. & Usova, L. V. (1989) *Geologiya i geofizika* **30,** 1–19.
44. Girnis, A. V., Stachel, T., Bulanova, G. P., Harris, J. W. & Phillips, D. (1999) in *Proceedings of the VII International Kimberlite Conference*, eds. Gurney, J. J., Gurney, J. L., Pascoe, M. D. & Richardson, S. H. (Red Roof Design, Cape Town, South Africa), Vol. 1, pp. 247–254.
45. Pearson, D. G., Boyd, F. R., Haggerty, S. E., Pasteris, J. D., Field, S. W., Nixon, P. H. & Pokhilenko, N. P. (1994) *Contrib. Mineral. Petrol.* **115,** 449–466.
46. Haggerty, S. E. (1986) *Nature (London)* **320,** 34–38.
47. Griffin, W. L. & Ryan, C. G. (1995) *J. Geochem. Explor.,* 311–337.
48. Bovenkerk, H. P. (1961) *Am. Mineral.* **46,** 952–963.
49. Sobolev, N. V., Sobolev, V. N., Snyder, G. A., Yefimova, E. S. & Taylor, L. A. (1999) *Intern. Geol. Rev.* **41,** 129–140.
50. Moore, R. O. & Gurney, J. J. (1985) *Nature (London)* **318,** 553–555.
51. McSckimin, H. J. & Andreatch, P. (1972) *J. Appl. Phys.* **43,** 2944–2948.
52. Fei, Y., Saxena, S. K. & Navrotsky, A. (1990) *J. Geophys. Res.* **95,** 6915–6928.
53. Saxena, S. K., Chatterjee, N., Fei, Y. & Shen, G. (1993) *Thermodynamic Data on Oxides and Silicates* (Springer, New York).
54. Slack, G. A. & Bartram, S. F. (1975) *J. Appl. Phys.* **46,** 89–98.
55. Dawson, J. B. & Smith, J. V. (1975) *Nature (London)* **254,** 580–581.
56. Boyd, F. R. & Finnerty, A. A. (1980) *J. Geophys. Res.* **85,** 6911–6918.
57. Shee, S. R., Gurney, J. J. & Robinson, D. N. (1994) *Contrib. Mineral. Petrol.* **81,** 79–87.
58. Zhang, L. B., Utsumi, W. & Liebermann, R. C. (1996) *Phys. Chem. Minerals* **23,** 1–10.